NeuroImage 276 (2023) 120197

Contents lists available at ScienceDirect

NeuroImage

journal homepage: www.elsevier.com/locate/neuroimage

Cortical maps of somatosensory perception in human

Seokyun Ryun[a], Minkyu Kim[b], June Sic Kim[c], Chun Kee Chung[a,c,d,*]

[a] Neuroscience Research Institute, Seoul National University Medical Research Center, Seoul, Korea
[b] Department of Cognitive Sciences, University of California Irvine, Irvine, USA
[c] Department of Brain & Cognitive Sciences, Seoul National University College of Natural Sciences, Seoul, Korea
[d] Department of Neurosurgery, Seoul National University College of Medicine, Seoul, Korea

ARTICLE INFO

Keywords:
Somatosensory cortex
Direct cortical stimulation (DCS)
Electrocorticography (ECoG)
Somatosensation
Movement

ABSTRACT

Tactile and movement-related somatosensory perceptions are crucial for our daily lives and survival. Although the primary somatosensory cortex is thought to be the key structure of somatosensory perception, various cortical downstream areas are also involved in somatosensory perceptual processing. However, little is known about whether cortical networks of these downstream areas can be dissociated depending on each perception, especially in human. We address this issue by combining data from direct cortical stimulation (DCS) for eliciting somatosensation and data from high-gamma band (HG) elicited during tactile stimulation and movement tasks. We found that artificial somatosensory perception is elicited not only from conventional somatosensory-related areas such as the primary and secondary somatosensory cortices but also from a widespread network including superior/inferior parietal lobules and premotor cortex. Interestingly, DCS on the dorsal part of the fronto-parietal area including superior parietal lobule and dorsal premotor cortex often induces movement-related somatosensations, whereas that on the ventral one including inferior parietal lobule and ventral premotor cortex generally elicits tactile sensations. Furthermore, the HG mapping results of the movement and passive tactile stimulation tasks revealed considerable similarity in the spatial distribution between the HG and DCS functional maps. Our findings showed that macroscopic neural processing for tactile and movement-related perceptions could be segregated.

1. Introduction

Somatosensory information for movement and tactile sensations is crucial for our daily lives as well as survival. They enable localization and characterization of somatosensory information and movement-related somatosensory feedback about location and status of our body and limbs (Dijkerman and de Haan, 2007). As a major neural entry of somatosensory information in the cortex, the primary somatosensory cortex (S1) has an indispensable role in early processing for somatosensation. Because lesions in S1 can cause devastating perceptual disorders, numerous studies have focused on the perceptual relevance of neuronal activities in S1. For several decades, however, converging evidence has suggested that perceptual processing for somatosensation is a neural orchestration of sensory-related networks in our brain, including S1 and other sensory-related cortical areas (Caruana et al., 2018; Delhaye et al., 2018; Dijkerman and de Haan, 2007; Platz, 1996; Preusser et al., 2015). Many studies have indicated that lesions other than S1 also cause severe perceptual disorders including tactile agnosia (Reed et al., 1996), impairments in tactile discrimination (Murray and Mishkin, 1984) and various sensorimotor-related deficits (Freund, 2001). Moreover, a recent human intracranial recording study indicated that more than 10% of the cortical areas, including the S1 and surrounding fronto-parietal areas, are activated during a single median nerve stimulation, although their perceptual relevance remains to be elucidated (Avanzini et al., 2016).

Since the major roles of tactile and movement-related sensations in human behavior are functionally different, several theoretical studies have proposed that there may exist two different cortical networks depending on their perceptual functions (Dijkerman and de Haan, 2007; Freund, 2001; Gardner, 2010). It has been suggested that the first network, from the S1 via the secondary somatosensory cortex (S2), surrounding the inferior parietal areas and posterior parietal cortex (PPC) to the insula is closely related to perceptual process of tactile information, object recognition and discrimination (Preusser et al., 2015; Reed et al., 2005), whereas the second network, from S1 to PPC (either directly or via S2) is tightly linked to movement-related processing including reach and grasp (Buneo and Andersen, 2006; Delhaye et al., 2018; Westwood and Goodale, 2003). Additionally, in monkey studies, the majority of neurons in the superior parietal lobule responded to joint movement during passive somatosensory stimulation, and the anterior

* Corresponding author at: Department of Neurosurgery, Seoul National University College of Medicine, 103 Daehak-ro, Jongno-gu, Seoul 03080, South Korea
E-mail address: chungc@snu.ac.kr (C.K. Chung).

https://doi.org/10.1016/j.neuroimage.2023.120197.
Received 13 September 2022; Received in revised form 5 May 2023; Accepted 25 May 2023
Available online 26 May 2023.

part of the superior parietal lobule was involved in hand/foot manipulation (Breveglieri et al., 2006; Gamberini et al., 2018). However, the specific cortical areas and functional roles of the proposed networks are still controversial (Dijkerman and de Haan, 2007; Disbrow et al., 2003). Furthermore, to the best of our knowledge, no electrophysiological study has addressed this macroscopic cortical-level segregation by directly comparing the two distinct somatosensations from the perspective of large-scale cortico-cortical networks, especially in humans.

In human study, direct cortical stimulation (DCS) and electrocorticography (ECoG) recording have been standard techniques to assess this issue. DCS provides a unique opportunity to identify the somatosensation-related areas directly with a wide coverage of the cortical surface in humans. Although its robustness is not as good as that of intracortical microstimulation (ICMS) (Armenta Salas et al., 2018; Flesher et al., 2016; Hiremath et al., 2017), DCS on the somatosensory-related area often elicits a specific somatosensation and the human subject can verbally report the quality of the sensation (Balestrini et al., 2015). However, DCS does not always guarantee that the elicited perception is actually caused by DCS-induced neuronal activation in that area, given that DCS can potentially affect a nearby cortico-cortical fiber tract, leading to neural activation of other cortical areas. Conversely, ECoG recording during somatosensory stimulation immediately detects ongoing neural activations in the located region; however, it is difficult to confirm that these neural activities are directly involved in the somatosensory perception itself.

Taking these issues together, the present study combines DCS data for eliciting somatosensory perception and high-gamma (HG) band mapping data during various somatosensory-related tasks by using the same neuroimaging techniques in humans. It is known that HG activity is a robust in ECoG recording. It may contain detailed information about tactile sensation (Ryun et al., 2017b). It might be closely related to the ongoing spiking activity (Ray et al., 2008). We also show that large-scale cortical network for somatosensation could be segregated depending on their functions by assessing the spatiotemporal differences in DCS responses and HG activation patterns during movement-related and tactile tasks from 51 (for DCS mapping) and 46 (for HG mapping) patients with intractable epilepsy.

2. Materials and methods

2.1. Patients

For the DCS study, we retrospectively investigated 238 patients (116 female, 27.13 ± 12.01 y; mean ± standard deviation; 12,110 electrodes from 262 hemispheres, left = 133, right = 129) who underwent implantation of subdural electrodes for epilepsy monitoring and functional cortical mapping with DCS from the database of Seoul National University Hospital between January 2005 and December 2018 (618 patients). Pediatric patients under the age of 12 and patients with poor resolution of post-operative computed tomography (CT) images or with large tissue defects were excluded from the analysis (30 patients). Among them, 111 patients (46.6%) reported sensorimotor-related experiences. Finally, fifty-one patients (21.4%) who reported sensory-only experiences without objective motor symptoms were included for further analysis.

For the four-dimensional (space and time) cortical HG mapping, 46 patients with intractable epilepsy participated in this study (17 left hemisphere; 25 right hemisphere; 4 bilateral). Among them, twenty patients (1256 electrodes), 22 patients (1388 electrodes) and 29 patients (1696 electrodes) participated in the hand grasping/elbow flexion, texture stimulation and vibrotactile stimulation tasks, respectively. The subdural conventional and high-density ECoG electrodes (Ad-tech Medical Instrument and PMT Corp.) had diameters of 4 and 2 mm with an inter-electrode distance of 10 and 4 mm, respectively. Pre-operative magnetic resonance (MR) and post-operative CT images were obtained from each patient. All experimental procedures were approved by the Institutional Review Board of Seoul National University Hospital (1905–156–1035 & 1610–133–803). All patients who participated in the experiments provided written informed consent before participation.

2.2. Direct cortical stimulation

Functional cortical stimulation mapping was performed as part of the clinical procedure. DCS was delivered with a GRASS S12 or S12X cortical stimulator (Natus, Warwick, RI, USA). During the pre-surgical functional mapping, 0.5 to 16.5 mA of bipolar electrical stimulation was delivered to each electrode (pulse train duration of 5 s; pulse width of 0.3 ms; stimulus frequency of 50 Hz with alternating polarity). Patients were asked to freely report verbally any abnormality they feel. Only verbal feedbacks without actual motor activity were included as subjective sensations and were considered in this study. Patients were not aware of when or where stimulation was applied. Stimulated electrodes eliciting after-discharge or other pathological responses were discarded. Additionally, intracerebral electrodes located on the white matter were excluded from further analysis. Among the fifty-one patients, DCS was performed by using two adjacent electrodes (23 patients), or choosing one reference electrode far from the target one (1 patient), or both (27 patients). For DCS using two adjacent electrodes, each electrode site was counted separately because one electrode was usually stimulated at least twice with different pairs of adjacent electrodes. If the patient reported the same sensory experience when the same site is stimulated with different types of stimuli (neighboring and reference-based bipolar stimulations), this case was considered once. Some patients reported sensory reports differently depending on the type of stimulation. These sensory reports were recorded as different cases (14 electrodes). We finally devised a dataset containing 297 verbal reports from 283 different electrode positions from 51 patients.

2.3. Classification of verbal feedbacks

The verbal reports were classified by the location of sensation and by the quality of the sensation. The locations of the sensations were categorized into 6 categories: (i) hand/finger and arm; (ii) face and head; (iii) lips; (iv) tongue; (v) torso including front, back, shoulder, neck and trunk; and (vi) leg and foot. The qualities of the sensations were initially categorized into 6: (i) moving sense and other movement-related sensations; (ii) tingling; (iii) electrical; (iv) paresthesia or numbness; (v) pressure; (vi) et cetera. Additionally, to compare the movement-related and tactile sensations, we merged (ii) to (v) into one category.

2.4. Localization of the electrodes

Electrode positions were obtained from co-registration of the pre-operative MR and the postoperative CT images using the CURRY software (version 7.0; Compumedics Neuroscan). These electrode positions of individual coordinates were subsequently converted to the MNI coordinate system and projected to the hemisphere-unbiased 3D MNI surface template consisting of 81,924 nodes, constructed by the CIVET pipeline (ver. 1.1.7, MNI) (Kim et al., 2005; Lyttelton et al., 2009). This method for generating 3D surface template was also used to construct three- and four-dimensional functional maps. For each electrode position, the nearest node on the cortical surface was chosen based on the Euclidean distance. To construct probabilistic maps, we used a 5 mm circular mask with binary values based on the geodesic distance from each electrode position at the individual level, and these masked maps were then summed across all patients. The electrodes located in the right hemisphere were projected to the corresponding nodes in the left hemisphere because the electrode sampling densities of some experimental conditions were sometimes relatively low in the opposite hemisphere.

In this study, therefore, we did not focus on the hemispheric differences, but on the spatial distribution within the hemisphere.

To identify the brain region of each node, we used the automated anatomical labeling (AAL) atlas for our template surface. Additionally, we constructed the surface map of Brodmann's area (BA) by directly comparing with previous studies (Papademetris et al., 2006; Xia et al., 2013). The anatomical boundaries between the dorsal and ventral premotor cortices (BA 6) and the S2 area were determined according to the literature (Eickhoff et al., 2006; Tomassini et al., 2007). In this study, the OP1 (opercular region) and the posterior part of the OP4 were defined as the S2 area.

2.5. Apparatus

For the texture stimulation, we designed custom-made disk/drum type stimulators, driven by ultrasonic motors (USR60E3N; Shinsei Corp.). The specification for the disk type stimulator is described in the literature (Ryun et al., 2017b). The drum-type texture stimulator, an advanced version compared to the disk type one, was designed to pseudo-randomly deliver eight different textures with different normal forces (light touch to several hundred gw). To control the accurate horizontal movement of the texture drum, we used a geared encoder motor and photo interrupter detecting the boundary of the horizontal shaft. To measure the normal force on the skin during the stimulation, a small load cell was attached on the plastic finger rest. In this study, the rotating speed of the drum was 10 rpm, with a diameter of 190 mm, a stimulus duration of 1.5 s, a texture width of 25 mm, and a normal force of 38 ± 17 g wt. (mean ± SD).

For the vibrotactile stimulation, we designed a custom-made pin-point piezoelectric actuator and magnetic vibrator. A detailed description of the piezoelectric actuator is in our previous study (Ryun et al., 2017b). The pin-point magnetic vibrator, driven by a Mini-shaker (model 4810; Brüel and Kjær), was designed for various vibrotactile and light pressure stimulations. To stimulate a fingertip, a long plastic pin (2 mm in diameter; 100 mm in length) was mounted on the top of the Mini-shaker. The plastic pin and Mini-shaker were shielded by barrel-shaped stainless steel and sound absorbing material for minimizing electromagnetic artifacts and stimulus-related auditory noise, respectively. Only the tip of the plastic pin was exposed to the top of the barrel lid with minimal indentation of the skin.

2.6. Tasks

Twenty patients (10 female, 16–40 years) performed self-paced, fully voluntary hand grasping and elbow flexion movements, as described in previous studies (Ryun et al., 2017a, 2014). Patients were instructed to grasp/flex their hands/arms with no object at approximate intervals of 5 to 10 s. Note that these motions are less related to the goal-directed movement. To determine the onset/offset of each movement, we recorded electromyogram (EMG) from the opponens pollicis for hand grasping and from the biceps brachii for elbow flexion tasks. The tasks were video-recorded for monitoring the performance and sequence of the movement. The mean durations of each task were 2.34 ± 1.08 s and 3.12 ± 1.20 s for hand grasping (1880 valid tasks) and elbow flexion (1620 valid tasks), respectively.

Texture and vibrotactile stimulation tasks have previously been described in detail (Ryun et al., 2017b). Twenty-two patients (10 female, 16–44 years) performed texture stimulation tasks. To do this, we used customized disk-type (for 17 patients) and drum-type (for 5 patients) texture stimulators. For the disk-type texture stimulator, two different textures (2 mm grid and <50 μm fine textures) were pseudo-randomly delivered to the contralateral index finger (80 trials per each texture). For the drum-type texture stimulator, eight different textures were pseudo-randomly delivered, but we considered only two textures (2-mm grid and <50 μm fine textures) for consistency (30 to 32 trials per each texture). The stimulus period was 1.5 s for both stimulators. Note that there was no static indentation during the resting period.

For twenty-nine patients (12 female, 16 to 58 years), pin-point, sinusoidal vibrotactile stimuli were delivered to the contralateral index finger by a customized piezoelectric (22 patient; 1 s of stimulus duration; 50 trials per each condition) or magnetic vibrotactile stimulator (7 patients; 1.5 s of stimulus duration; 40 trials per each condition). We delivered various vibrotactile stimuli including 5 to 400 Hz sinusoidal and combined (flutter + vibration) stimuli, but we used 33 or 35 Hz (flutter; 120 μm for 33 Hz, 180 μm for 35 Hz) and 350 or 400 Hz (vibration; 60 μm for 350 Hz, 90 μm for 400 Hz) stimuli for further analysis given our previous finding (Ryun et al., 2017b). Throughout experiments, a voltage-displacement amplitude calibration procedure was performed at each stimulus frequency by using a Laser-Doppler Vibrometer (LDV; model AT3600, GRAPHTEC Corp., Japan). Note that we conducted all experiments only when the patients' electrode grids were located on the sensorimotor-related areas. Therefore, we were able to obtain maps with a relatively high sampling density in these areas.

2.7. Data recording and processing

ECoG data were recorded with the 128-channel Natus Telefactor (Telefactor Beehive Horizon with an AURA® LTM 64 & 128 channel amplifier system, Natus Neurology, West Warwick, RI, USA) or the Neuroscan (Neuroscan, Charlotte, NC, USA) or Neuralynx ATLAS (Neuralynx, Bozeman, MT, USA) systems at 200, 400, 1000, 1600 or 2000 Hz with analog anti-aliasing filtering ranging from 0.1 to 80, 150, 200, 400, and 500 Hz, respectively. ECoG channels, which show abnormal fluctuations due to technical problems, were preferentially excluded from further analysis. The data were re-referenced to a common average reference (CAR) and then notch-filtered with a zero-phase-lag infinite-impulse response (IIR) filter to remove systematic noise at 60 Hz and related harmonics. Data epoching was performed with a window of −2 to 3 s of movement or stimulus onset. Epoched data from all electrodes were decomposed into time-frequency representation using the complex Morlet's wavelet transform (seven cycles). Transformed data were squared and then normalized by the mean and standard deviation of the baseline period (−1.5 to −0.5 s of stimulus/task onset). The HG power ranging from 50 to 150 Hz frequency band (except one patient (50 to 80 Hz), due to a low sampling rate) was extracted with 50 ms bins. The binned HG power was compared with that of the baseline period using a *t*-test. Finally, t-values of high-gamma activities were extracted from electrodes of each patient.

To test the hemispheric predominance of responsive electrodes in tactile condition (Supplementary Figure 3 and 4), a chi-squared test (responsive-non responsive vs. left-right hemispheres) was performed. To construct Fig. 2D, we first tested whether distributions of responsive electrodes were different between each condition. To do this, we performed Fisher's exact test because the expected values of electrodes in four areas (66%) were less than five. We then performed a chi-squared test to confirm the significant difference in responsive electrode distribution between dorsal and ventral areas of the parietal lobe.

2.8. Mapping on the brain

There is no gold-standard method to combine electrodes from large dataset of ECoG, but some previous studies have provided ways to combine them (Avanzini et al., 2016, 2018; Nakai et al., 2017). We referenced and modified the method by Avanzini, et al. to construct three- or four- dimensional functional maps.

To build a four-dimensional functional map across all patients, we initially generated t-value (which was extracted in the previous section) based functional map of each patient. Because the sampling densities of each brain region were inhomogeneous, we defined partial amplitude *P* by adjusting the t-values of each electrode using the following

equations:

$$P_{i,j} = \begin{cases} 0 \; if \; s_{i,j} = 1 \\ \frac{t_{i,j}}{s_{i,j}} \; otherwise \end{cases} ; \quad i = 1, \ldots, M; j = 1, \ldots, N_i$$

$$s_{i,j} = 1 + \sum_k A_{i,j,k}; \; k = 1, \ldots, i-1, i+1, \ldots, M,$$

where t is the t-value from each electrode; s is the spatial weight; P is the partial amplitude; M is the number of patients; N_i is the number of electrodes of each patient i, and $A_{i,j,k}$ is the number of electrodes of the other patient k within a 5 mm geodesic distance from the target electrode j of patient i. Note that the partial amplitude P is 0 if there is no surrounding electrode (within 5 mm) from other patients (the value of this electrode was discarded to minimize false-positive ratio because the value only depends on single electrode).

For each node indicating the electrode location, the values of the target and surrounding nodes (within 5 mm geodesic distance) were masked with the partial amplitude of each electrode. To reduce the edge effect at the boundary of the mask, a linear interpolation based on the path length was performed for all nodes (effective distance from target node: 5 to 10 mm). Finally, the masked and interpolated partial amplitudes of all nodes were summed across all patients (overall amplitude).

Testing whether the calculated overall amplitude was significant could not be addressed by conventional statistics. Therefore, we performed simulation method to figure out their significance indirectly. First, nodes with overall amplitude exceeding a given threshold in at least three time bins within 0 to 1 s of the stimulus/task onset were considered as significant ones (Avanzini et al., 2016). This criterion was also used for calculating three-dimensional HG significance maps. To determine the significant threshold level, we repetitively simulated the whole procedure (calculating partial amplitude, finding neighboring electrodes, spatial masking and summation) above (1000 iterations) with the same electrode distributions used for calculating the 'real' dataset for a pseudo random z-value (from standard normal distribution because t-values of baseline period almost perfectly followed standard normal distribution (Supplementary Fig. 1 (top) and were temporally random due to jittering effect of stimuli/tasks) time series of each node, as increasing the threshold level (Supplementary Fig. 1 (bottom)). The critical point when the probability that all nodes are completely rejected (no false positive) by the given threshold is above 95% from 1000 iterations was determined as the significant threshold level (generally, threshold Thr = 1.76-1.79, we selected Thr = 1.8 as the threshold of all conditions for consistency). We did not perform multiple comparison corrections in this simulation analysis because our simulation procedure did not include any multiple comparison. To construct Fig. 6B, we calculated Pearson's correlation between conditions for all nodes (n = 81,924). We used Fisher's Z transform-based statistical test to test the significance between two correlation coefficients.

2.9. ROI-based analysis

To construct Fig. 6A, electrodes with $p < 0.0025$ (Bonferroni corrected for 20 comparisons) in at least three consecutive time bins (50 ms) during 0 to 1 s of stimulus onset at each ROI were selected (Avanzini et al., 2016). To compare proportions of responsive electrodes in Fig. 6A, a chi-squared test was performed for each pair (movement-related vs. tactile) in various cortical areas. For multiple comparison, we performed Bonferroni correction.

To confirm the temporal difference in areas shown in Fig. 7 (and Movie 1) was significant, we also performed ROI-based HG time series analysis. For this analysis, electrodes within 30 mm in diameter were initially chosen in each ROI based on the result in Fig. 6. Then we excluded electrodes located outside the corresponding Brodmann areas (e.g., if electrodes from the dSMG ROI were located in area 7, we discarded them). The average HG time series was calculated in the electrodes selected in each ROI (Fig. 8). We used independent two-sample t-test to test the significance between two time points (movement vs. tactile) in each ROI. False discovery rate (FDR) correction was performed for multiple comparisons.

To analyze the peak delays of HG activities from several ROIs, we initially extracted electrodes of each ROI in the surface template and then re-calculated the t-value time-series of each electrode with 20 ms bins (to increase time resolution) using the same method described above. To reject electrodes with non-significant HG peaks, only electrodes with $p < 0.001$ (Bonferroni corrected for 50 comparisons) in at least three consecutive time bins during 0 to 1 s of stimulus onset were selected. This threshold (p = 0.001) was only used for constructing Fig. 9. To construct Fig. 9, the t-values of each selected electrode in the same ROI were averaged across all patients.

3. Results

3.1. DCS mapping

In this study, we included epilepsy patients who reported somatosensations without actual movement during the DCS functional mapping procedure (51 of 238 patients). Overall, we collected 297 verbal reports from 283 different electrode positions. Patients reported various somatosensory experiences including movement-related (joint move (12.5%), tremor (25.5%) and other muscle sensations (8.1%)), tingling (20.2%), electrical (13.1%), paresthesia or numbness (9.1%), pressure (0.7%), and unclassified (10.8%) sensation at various body parts (finger/hand/arm = 55.4%, face/neck = 18.3%, tongue/oral/lip/throat = 17.0%, leg/foot = 4.3%, torso/front/back = 5.0%). We divided them into three categories: (i) movement-related sensations, (ii) tactile sensations, and (iii) unclassified. All sensations were elicited on the contralateral side of the stimulus site. Pain (unclassified) was reported for only one electrode (located on the S2) among all the electrodes of the exposed cortical sites. Because the sampling density of the medial parts (inside the inter-hemispheric and Sylvian fissures) was relatively low (< 5% of the total responsive electrodes), we focused on the exposed cortical sites. All responsive electrodes eliciting somatosensory experiences were projected to the hemisphere-unbiased MNI surface template (Supplementary Fig. 2 for the brain atlas of our surface template).

Artificial somatosensations were elicited not only from conventional somatosensory-related areas such as the S1 (BA 3, 1 and 2) and S2 but also from a widespread network including the inferior parietal lobule (IPL), superior parietal lobule (SPL), and premotor cortex (PM) (Fig. 1A). The highest proportion of responsive electrodes was present in the S1 (40.4%), followed by primary motor cortex (M1; 15.4%), SPL (13.9%), IPL (10.0%), PM (9.62%) and S2 (4.62%). Interestingly, distribution of the electrode locations with the elicited somatosensation showed distinct spatial difference depending on the quality of the somatosensation. DCS on the dorsal part of the parietal area, including the SPL, mainly induced a movement-related somatosensation, whereas that on the ventral part of the parietal area, including the S2 and the IPL, generally elicited a tactile sensation (Figs. 1B and C; chi-squared test, $\chi^2 = 7.79$, $p = 0.005$). Note that no movement-related sensation was reported in the posterior S2 and adjacent vIPL regions even though twenty-three responsive electrodes were located on these areas. Additionally, a significant right hemispheric predominance in tactile sensation condition was found in the S2 and vIPL (chi-squared test, $\chi^2 = 8.63$, $p = 0.003$) (Supplementary Figs. 3 and 4). However, it is possibly due to the fact that clinicians mainly focus on language function during DCS on the inferior parietal area of the dominant hemisphere; thus, further investigation is needed to verify this issue. In this study, we focused on the spatial distribution within the hemisphere.

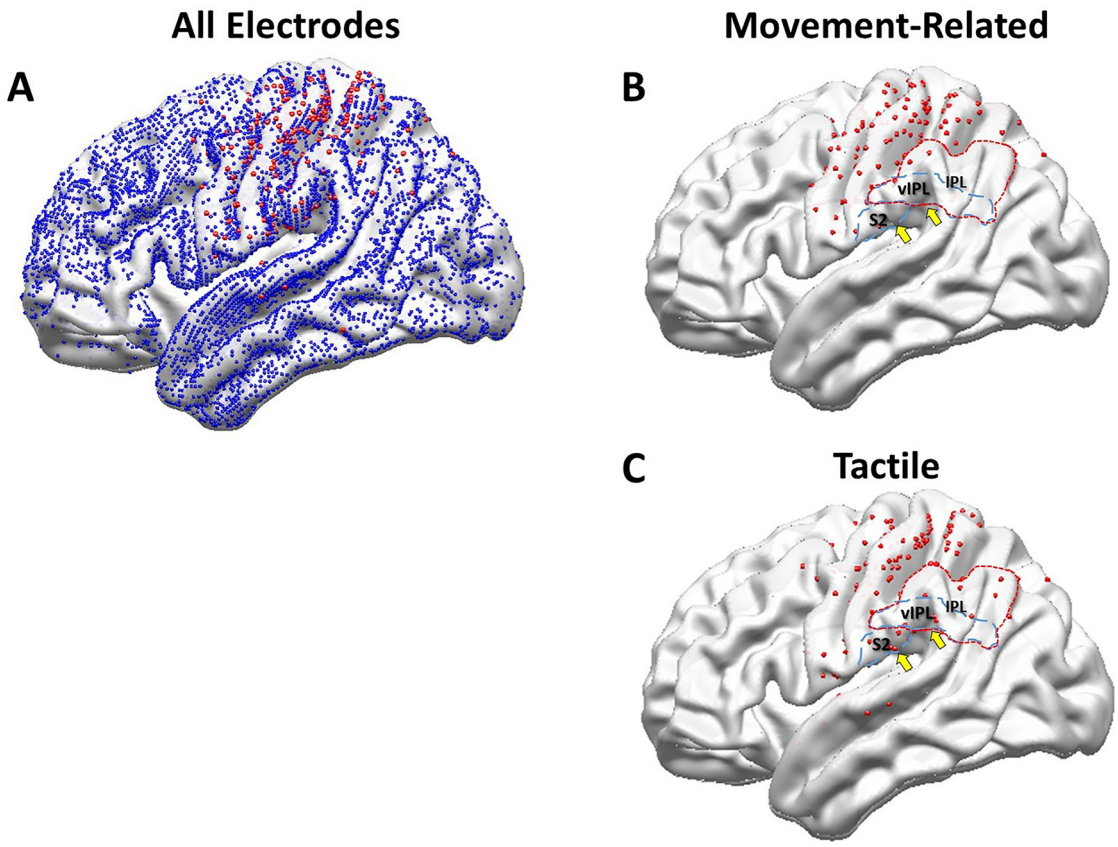

Fig. 1. 3-D DCS functional maps. (A) Electrode locations eliciting somatosensation during DCS from entire body parts regardless of sensory quality (red dots). Blue dots indicate electrodes with negative responses. The electrodes located in the right hemisphere were projected to corresponding sites in the left one. (B and C) Electrode locations whose stimulation elicits (B) movement-related and (C) tactile sensations. Yellow arrows indicate the area S2 and ventral IPL. The red dotted line indicates the IPL.

Next, we focused on the elicited sensation of the finger/hand/arm areas for detailed quantification and direct comparison with further HG results below. Note that the corresponding somatotopy of these body parts in the S1 is sufficiently far from the ventral fronto-parietal area including the S2, vPM and vIPL, avoiding spatial ambiguity due to the intrinsic resolution of our approach. As mentioned above, in the finger/hand/arm condition, the difference in the spatial distribution between movement-related and tactile sensations was prominent in the dorsal and ventral fronto-parietal areas (Figs. 2A and B). Beyond the primary sensorimotor area, movement-related sensations were mostly elicited by stimulation on the SPL and dPM, whereas that on the IPL, vPM and S2 almost exclusively generated tactile sensations (Fig. 2D; Fisher's exact test for six regions, $p = 0.0059$; chi-squared test for the dorsal (SPL and dPM) and ventral (S2, vPM and vIPL) areas, $\chi^2 = 12.49$, $p = 0.0004$; Supplementary Table 1). Additionally, the stimulation on the SPL induced both sensations with the highest proportion, suggesting that the SPL is involved in both tactile and movement-related somatosensations.

3.2. Three and four-dimensional HG mapping

Although our DCS results indicate that there is a distinct spatial difference between movement-related and tactile perception, it is possible that artificial somatosensation was induced by top-down streams from non-primary areas. In the preliminary analysis, however, we observed significant HG activities during passive tactile stimulation from the electrode located on the non-primary areas, where the patient reported tactile sensation during DCS (Supplementary Fig. 5). To generalize this observation that these non-primary areas are actually activated by such sensations, we constructed three- and four-dimensional brain maps (Avanzini et al., 2016; Nakai et al., 2017, 2018) for actual movement and passive tactile stimulation tasks. Forty-six epilepsy patients participated in this study (20 patients for hand grasping and elbow flexion tasks (1256 electrodes), 22 for coarse/fine texture stimulation tasks (1388 electrodes for both conditions), and 29 for flutter/vibration stimulation tasks (1696 and 1650 electrodes, respectively)). Five patients participated in both tactile and movement tasks (304 electrodes). The sampled electrode maps indicate a sufficient coverage of the exposed cortical sites, especially the cortical crowns of the sensorimotor-related brain regions (Fig. 3). In contrast, the cortical areas of the medial side and frontal pole were poorly sampled, except for the supplementary motor area (SMA) and medial temporal lobe. The mean spatial weights, indicating the number of electrodes of other patients within a 5 mm geodesic distance from each electrode (see Method and Materials for detail), were 3.75 ± 2.21 (mean $\pm$ SD) for the movement tasks, 3.81 ± 2.05 for the texture stimulation tasks, and 4.58 ± 2.53 for the vibrotactile stimulation tasks. Additionally, those of the sensorimotor-related areas (S1, M1, S2, SPL, IPL, and BA 6) were 4.22 ± 2.25 for the movement tasks, 4.32 ± 1.97 for the texture stimulation tasks, and 5.33 ± 2.44 for the vibrotactile stimulation tasks.

Significant HG activities were observed in various cortical regions including the S1, M1, SPL, IPL, BA 6 ventral (vPM), BA 6 dorsal (dPM and SMA), and S2 within 0 to 1 s of the task onset. In both hand grasping/elbow flexion and coarse/fine texture conditions, the S1, M1, SPL and BA 6 areas were consistently activated, whereas HG activities in S2 and adjacent IPL (representing supramarginal gyrus, SMG) areas exhibited a marked difference between the two conditions (independent 2-sample *t*-test, $t = 4.88$, $df = 276$, $p = 1.78 \times 10^{-6}$; Figs. 4 and 7 and Movie 1, see also Movie 1–1). Unlike the result of the DCS mapping, the posterior part of the IPL (angular gyrus, ANG) showed less dominant HG activity under both conditions. Interestingly, strong HG activities in the

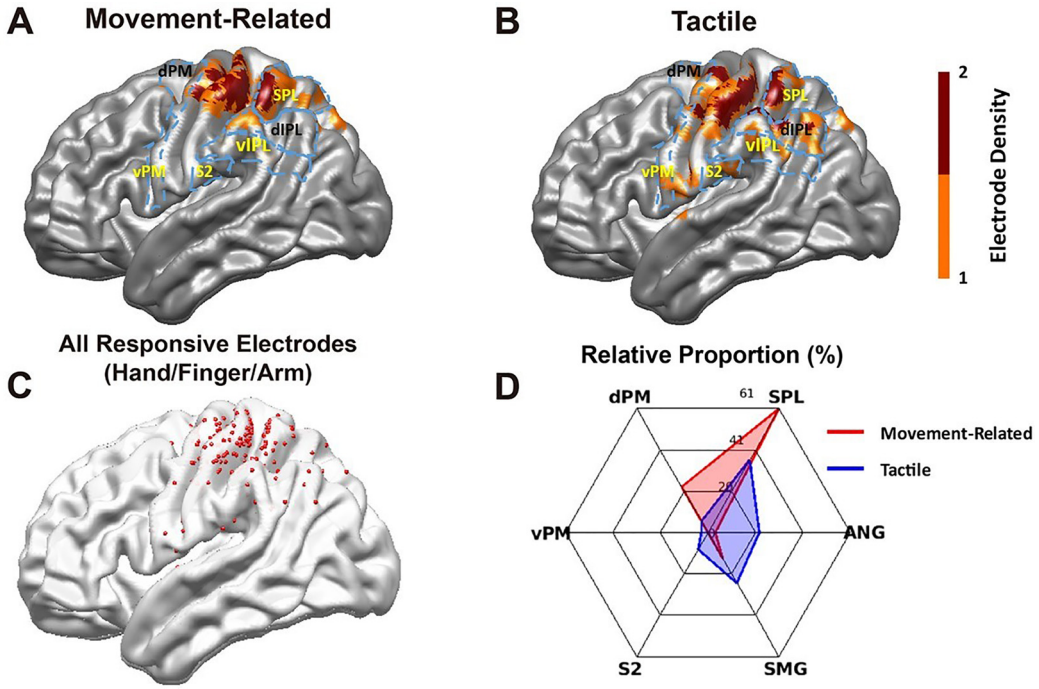

Fig. 2. 3-D DCS functional maps based on the quality of sensation ((A) movement-related and (B) tactile sensations). Corresponding body part of the maps is the hand/finger/arm. (C) Distribution of electrode where patients reported any somatosensation in hand/finger/arm. (D) Radar plots represent the relative proportion of the number of electrodes in each area for movement-related (red) and tactile (blue) sensations. Electrodes in S1 and M1 were excluded.

ventral PM were consistently observed regardless of the task conditions. In the texture conditions, significant HG activations were found in the medial part of BA 5, the medial part of S2 and insula regions, but these areas could not be compared with the movement conditions due to the low sampling density. We also found a weak but significant HG activity in the middle temporal region (MT), consistent with a previous finding (Avanzini et al., 2016).

Movie 1. Four-dimensional cortical maps of HG activities during movement (hand grasping and elbow flexion, top) and tactile stimulation tasks (coarse and fine texture conditions, bottom). Time = 0 (ms) indicates task onset. Only the significant regions were shown in red.

Similar tactile-specific spatial patterns were observed in the vibrotactile stimulation conditions (flutter and vibration), although the amount of change in HG activity under these conditions was relatively small (Supplementary Fig. 6). These distinct spatial patterns of the HG activities during the movement-related and tactile conditions were more apparent at the individual level (Fig. 5).

Given the inhomogeneity of electrode coverage of the cortex, it may be plausible that neural activity in some regions was largely dominated by one or two electrodes with very strong HG activity. Therefore, we investigated the proportion of responsive electrodes in each ROI across all responsive electrodes in two conditions (movement-related and tactile conditions). The ROI analysis revealed that the ventral SMG area showed significant differences in the proportion of responsive electrodes (electrodes with $p < 0.0025$ in at least three time bins (50 ms bins) from 0 to 1 s of the task onset) for each ROI between the two conditions (Fig. 6A, see also Supplementary Table 2).

The significant cortical area was much wider in the texture condition (number of significant nodes = 2267 in coarse texture, 1932 in fine texture, 1777 in hand grasping, and 1103 in elbow flexion), although the overall amplitude was greater in the hand grasping condition (mean overall amplitudes of all significant nodes = 3.49 ± 0.03 in coarse texture, 3.20 ± 0.03 in fine texture, 3.94 ± 0.05 in hand grasping, and 3.06 ± 0.03 in elbow flexion). The spatial distributions of the overall amplitudes were very similar between the coarse and fine texture stimulus conditions (spatial correlation $r = 0.94$). In contrast, the spatial correlations between the hand grasping/elbow flexion and texture stimulus conditions were relatively low (Fig. 6B). Additionally, the mean overall amplitudes (0 to 1 s of the stimulus onset) of the coarse texture condition from the sensorimotor-related areas were generally greater than those of the fine texture condition, except for the lateral part of S2, consistent with a previous finding (Ryun et al., 2017b).

Our four-dimensional mapping analysis revealed that significant somatosensory-related regions are activated with different temporal dynamics (Fig. 7, Movie 1 and 1–1). Early HG responses (within 100 ms of the task onset) were observed in the S1, M1, SPL, and dorsal IPL in both the movement-related and tactile conditions. The increased S1 HG activities gradually decreased until the end of the task but were still significant throughout the task. Additionally, a transient HG burst in the S1 was observed at the task offset, consistent with previous findings (Callier et al., 2019; Ryun et al., 2017b). Prominent spatial differences in HG activation between the two conditions were found after approximately 200 ms of the task onset. HG activations in the ventral part of the IPL became significant after 150 to 200 ms of the task onset in the tactile condition, and these activities appeared to gradually propagate into the lateral S2 area. In contrast, no dominant HG activity was observed within 400 ms of the task onset in the movement-related condition. Interestingly, significant HG activities in the vPM were consistently found regardless of the task conditions. In the tactile condition, HG activities in the S2 area became significant after 350 to 400 ms of the task onset, after which it lasted about 450 ms. In the hand grasping and elbow flexion condition, weak but significant S2 HG activities were observed after 500 to 550 ms and 1600 ms of the task onset, respectively. It might be due to the neural response of the isometric contraction period during hand grasping (300 to 400 ms after the task onset) and elbow flexion (1 to 1.2 s after the task onset).

We also investigated the ROI-based temporal dynamics of HG activity between movement and tactile conditions. The results indicated significant HG differences in power levels between the two conditions depending on the ROI (Fig. 8). The ventral areas (vSMG and vPM)

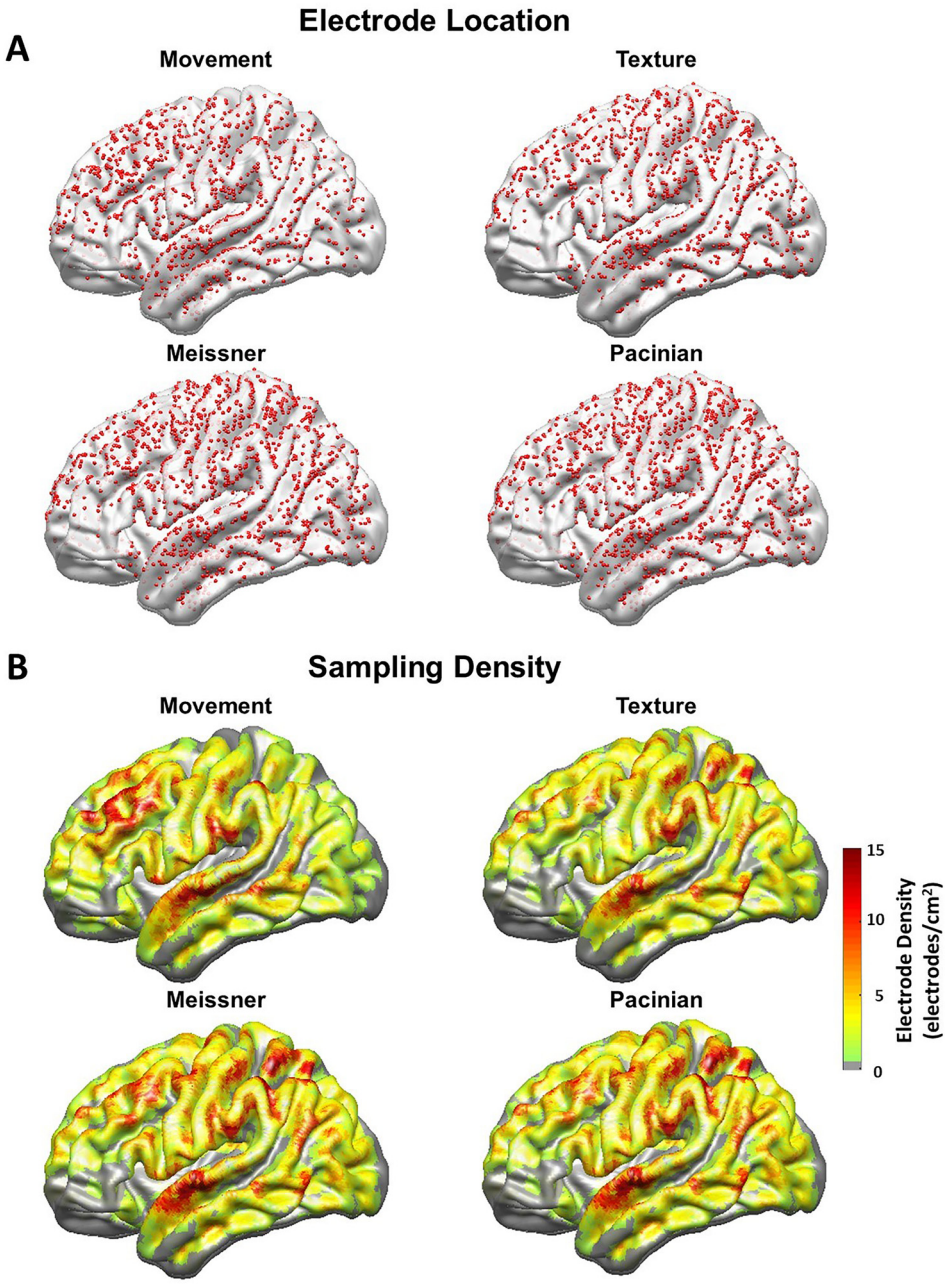

Fig. 3. Electrode locations and sampling densities. (A) Locations of all electrodes and (B) sampling densities of the electrodes, in each experimental condition. Note that electrodes covered most of the parietal lobe, M1, and PM regions with sufficient sampling densities.

showed strong activation in the tactile condition from 200 – 300 ms to 1 s, whereas strong and sustained activity was observed in dorsal (SPL and dPM) regions (500 ms to 2 s) in the movement condition. In the dSMG area, the tactile condition showed a narrow peak, but it rapidly decreased as in S1, whereas a gradual increase was found in the movement condition.

3.3. Neural characteristics among somatosensory-related areas

To quantify the temporal directionality of the HG activities among the identified regions, we investigated the peak latencies of the HG activities of each ROI. In this analysis, we focused on the texture condition because this condition activated the largest cortical area (compared to the movement condition) with a high signal-to-noise ratio (compared to the vibrotactile condition). Furthermore, the kinematics of the movement task change within a task period (i.e., grasp-isometric contraction-release) making it difficult to evaluate the exact timing of the HG peaks from the task onset.

The HG peak latency results revealed that somatosensory-related cortical areas were sequentially activated with different peak timings (Figs. 9 and Supplementary Fig. 7; Supplementary Fig. 8 for vibration). The HG activity in the S1 reached the peak first, followed by the SPL, dorsal part of IPL, ventral part of IPL, vPM, and S2. Interestingly, the HG peaks in the vPM and S2 showed high individual variability among the electrodes in each region, suggesting that neuronal population responses in these regions have unique characteristics such as a long-lasting HG activity compared to other regions (see Fig. 9A).

4. Discussion

In this study, we showed that somatosensation recruited a widespread somatosensory-related network in the cortex, including the S1 and S2. The cortical regions that elicited artificial somatosensation by DCS were tightly linked to the areas where strong HG activities were observed during actual somatosensory stimulation. Specifically, the results of the DCS and HG mapping revealed that functional cortical maps

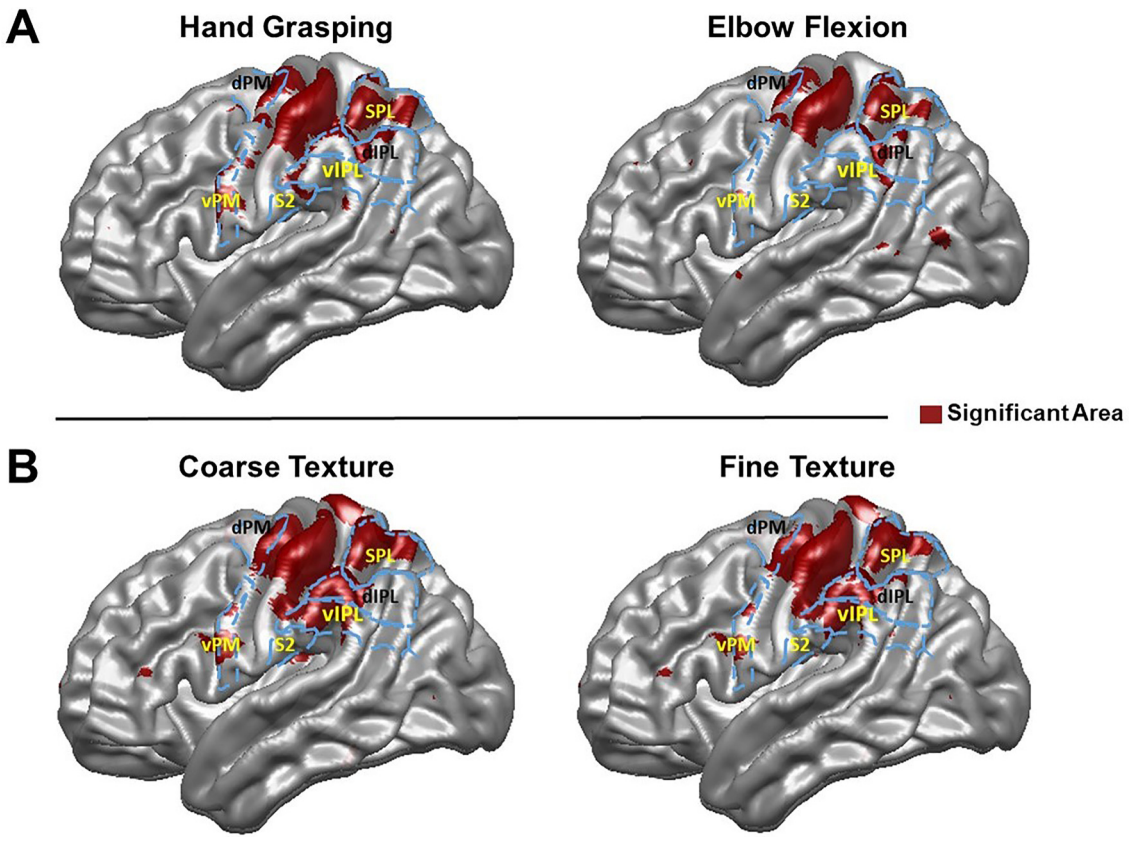

Fig. 4. Three-dimensional HG significance maps. (A) HG significance maps for hand grasping (left) and elbow flexion (right) conditions, and (B) those for coarse texture (left) and fine texture (right) conditions.

from these two approaches together show distinct spatial distributions depending on the somatosensory functions. In addition, somatosensory related cortical areas were sequentially activated with distinct temporal dynamics in each region. These results demonstrate that macroscopic neural processing for somatosensation has distinct hierarchical networks depending on their somatosensory functions.

4.1. Two networks of the somatosensory system

Several studies have proposed the existence of two distinct neural pathways which process the somatosensory perceptual functions (Delhaye et al., 2018; Dijkerman and de Haan, 2007; Gardner, 2010). One is from the S1 to the insula via the lateral parietal region such as the S2, representing the neural processing for perceptual recognition such as tactile perception. Another one is from the S1 to the dorsal parietal regions including the SPL, representing neural processing for movement-related perception. Although there are moderate differences in the areas of the two pathways and their interpretation compared to the previous suggestions, the present results indicate that there exist distinct networks reflecting neural processing for movement-related and tactile sensations in human cortex. In addition, the analysis results of the HG peak latency reveal the hierarchical process of the human somatosensory system among various somatosensory-related cortical regions including the S1, S2, SPL, IPL, and PM. Based on these findings, we suggest that a large-scale cortical network involving the S1, M1, SPL, PM and dorsal IPL reflects the stream for movement-related somatosensory processing, whereas the S1, M1, SPL, vPM, insula, S2 and adjacent IPL areas represents another network reflecting the stream for tactile-specific processing. Anatomically, these areas are densely connected with each other and project output to the frontal regions via the parieto-frontal pathway for decision or motor action (Delhaye et al., 2018; Dijkerman and de Haan, 2007).

The SPL was involved in both somatosensations; however, this area seems to be more related to the movement-related somatosensory processing. In the present study, DCS on the SPL mainly elicited movement-related somatosensations. Furthermore, previous lesion studies showed that lesions of the SPL cause mild deficits in tactile perception and discrimination but induce significant abnormalities in movement tasks (Padberg et al., 2010; Pause et al., 1989). In this study, the S2 and adjacent ventral IPL were not significantly involved in the movement-related somatosensory processing. Several studies suggested that the S2 is also related to movement-related somatosensation because this area also receives input from proprioceptive afferents and is connected to the cortical areas related to the movement control such as the PPC (Disbrow et al., 2003; Friedman and Murray, 1986). In human studies, the S2 is activated during passive movement and isometric contraction, and the S2 activation is modulated by movement (Huttunen et al., 1996; Lin et al., 2000; Xiang et al., 1997). In a magnetoencephalography (MEG) study, median nerve stimulation evokes both SPL and IPL activation (Huang et al., 2006). It might be due to the fact that median nerve stimulation usually induces tactile sensation and finger movement. Likewise, in a monkey study, neurons in the IPL respond during not only somatosensory stimulation, but also during movement (Rozzi et al., 2008). Additionally, the IPL is strongly linked to movement intention and illusion (Desmurget et al., 2009).

However, although the S2 receives proprioceptive information from the thalamus and other cortical regions, and the IPL is involved in movement processing, it is unlikely that the S2 and adjacent ventral IPL are significantly involved in the neural processing for movement-related somatosensation itself. First, in this study, no movement-related sensation was induced by DCS on these regions. All twenty-three somatosensory reports in these areas were tactile sensations. Furthermore, the HG activation of the S2 region became significant only during the isometric contraction phase inducing a strong tactile feedback in the hand grasp-

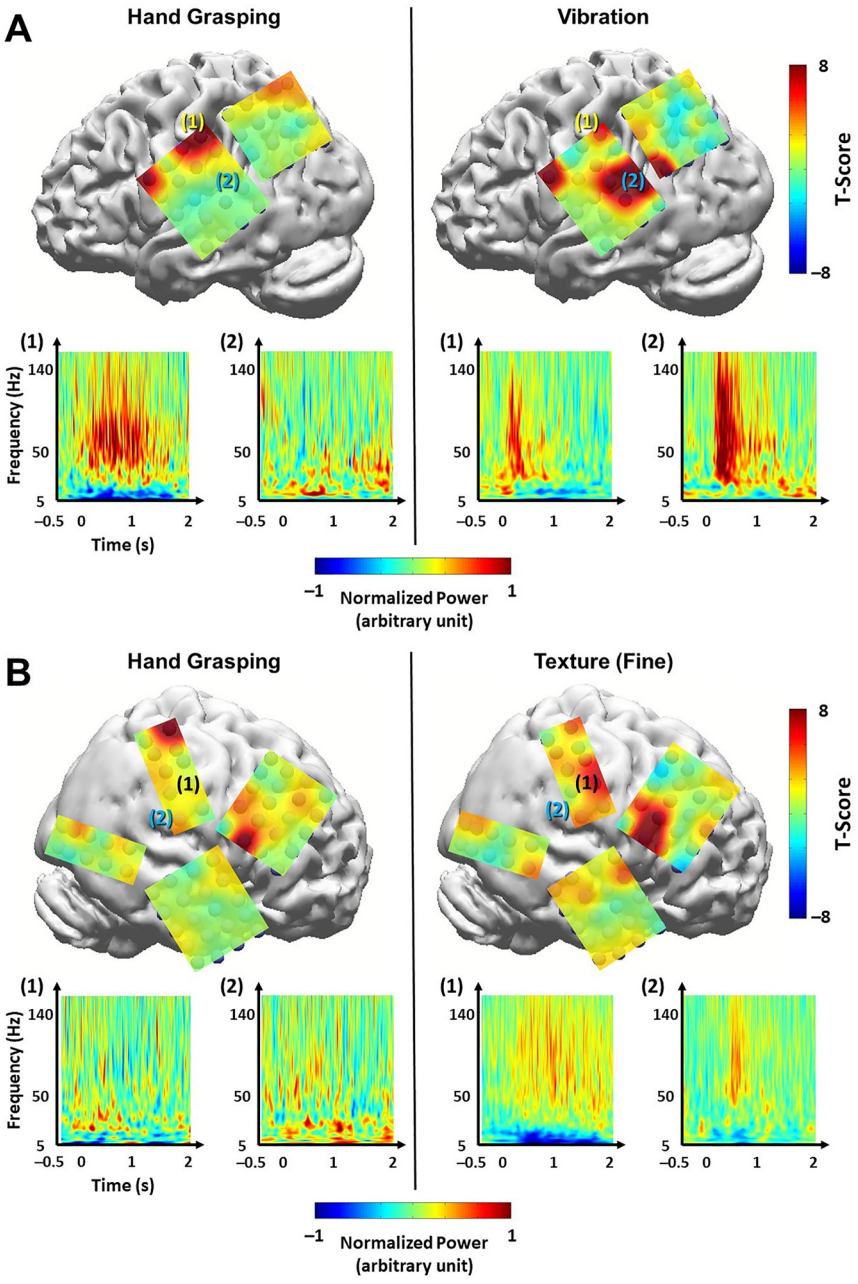

Fig. 5. Differences in HG activities at the individual level. (A) Topographical maps of the HG activities during hand grasping (left) and vibration stimulation (right). Areas (1) and (2) indicate the S1 and S2, respectively, and corresponding time-frequency representations of each area are shown at the bottom. Circles on the 3D brain structures indicate the locations of each electrode. (B) The same maps during hand grasping (left) and fine texture stimulation (right). Areas (1) and (2) indicate the IPL and S2, respectively. Corresponding time-frequency representations of each area are depicted below. Note that strong HG activities were consistently found in the vPM of both subjects, regardless of the task types.

ing and elbow flexion movements. Similar results have been reported in a human PET study (Grafton et al., 1996). These results imply that the received proprioceptive information in these regions are less related to the conscious perception for movement-related sensation. Rather, these areas may receive proprioceptive information not to consciously perceive the movement itself but to completely identify the object being touched, as complementary information. Second, several studies have shown that lesions in the S2 and IPL cause severe tactile deficits including tactile agnosia and impairment of texture and shape discrimination but do not affect the motor skills and proprioception (Murray and Mishkin, 1984; Reed and Caselli, 1994; Reed et al., 1996). Third, given the multimodal response characteristics and functional complexity of the IPL region, it is not surprising that the IPL is involved in both tactile perceptual processing and movement intention/recognition. Specifically, in the present study, the dorsal part of the IPL (near IPS) is involved in both movement-related and tactile sensations, whereas the ventral part of the IPL (near S2) is almost exclusively related to tactile one. This result indicates that although the neurons in the IPL often show multimodal responses, the relative proportion of preferred modality might be different depending on the locations within the IPL. This gradient-like organization in the PPC was also found in another human study (Heed et al., 2011).

The spatial differences between the two parieto-frontal somatosensory networks may be related to the anatomical characteristics of the cortico-cortical fiber tracts in humans: the superior longitudinal fasciculus (SLF) I and III. Conventionally, it is considered that SLF I, reciprocally linking the superior parietal region with the SMA and PM areas, may contribute to the motor behavior related to the body position, whereas the SLF III, connecting the vPM and SMG, may be related to the hand actions requiring higher-order somatosensory information (Kamali et al., 2014; Matelli et al., 1998; Rozzi et al., 2006; Schmahmann et al., 2008). Given the functional and anatomical similarities between the previous and current findings, these two pathways may be partially involved in somatosensory processing in a function-specific manner.

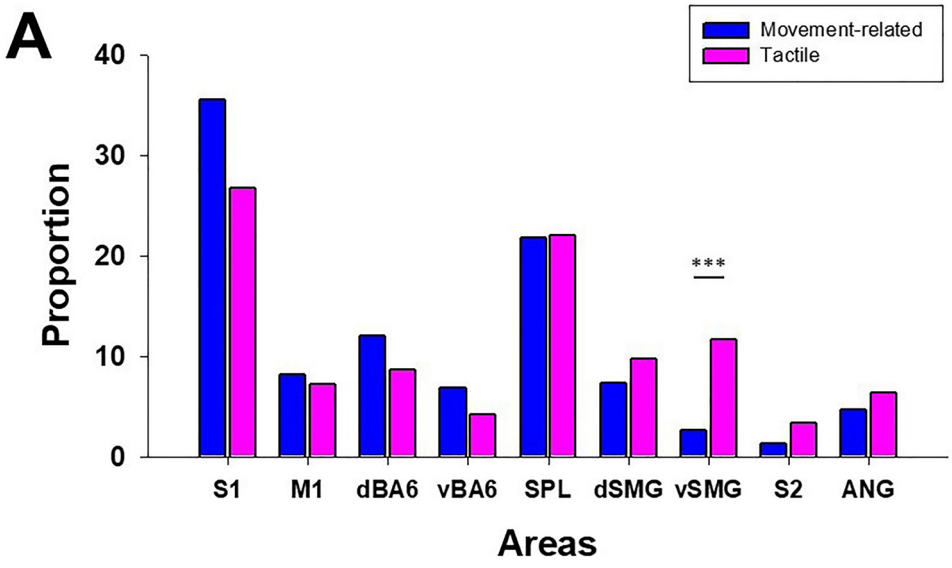

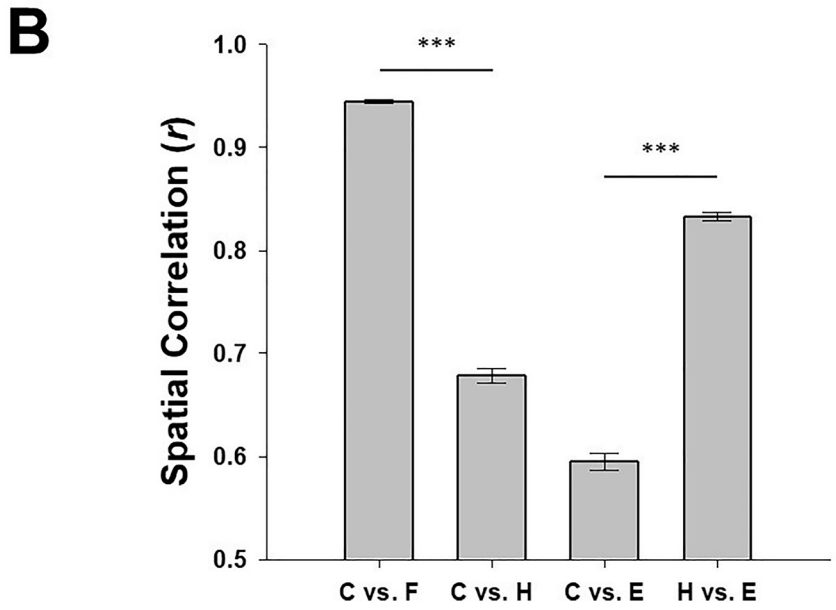

Fig. 6. Proportion of responsive HG electrodes and spatial correlations. (A) Difference in the proportion of responsive electrodes in each ROI across all responsive electrodes in each condition (movement-related (blue) and tactile (pink) conditions) (chi-squared test; *** significant pair; Bonferroni-corrected ($p < 0.01$) (dSMG = dorsal supramarginal gyrus; vSMG = ventral supramarginal gyrus). (B) Spatial correlation of HG significance maps between conditions. Error bar indicates the 99% confidence interval of r (*** $p < 0.001$) (C = coarse texture; F = fine texture; H = hand grasping; E = elbow flexion).

4.2. Functional role of the ventral PM

The present findings suggest that the vPM is critically involved in the neural processing for both tactile and movement-related information. Consistent with the current findings, a previous HG cortical mapping study reported significant HG activation in the vPM during median nerve stimulation, although its perceptual relevance was unclear (Avanzini et al., 2016). In monkey, the vPM is involved in the transformation of somatosensory information into action and in the tactile perceptual decision (Romo et al., 2004). In addition, several human studies have suggested that the vPM is involved in movement perception without somatosensory feedback by modulating the S1 and is activated during illusory somatosensory perceptions, 'the cutaneous rabbit' (Blankenburg et al., 2006; Christensen et al., 2007). In this study, we showed that DCS on the vPM induces artificial somatosensation, and this area is activated by various types of somatosensory stimuli. Given the present and previous findings, the vPM may be a cortical hub that performs both bottom-up and top-down somatosensory perceptual processing for tactile and movement-related information.

4.3. Limitations and perspective

Previous studies have indicated that there is a hemispheric predominance in somatosensory processing (Jancke et al., 2001; Naito et al., 2017; Stoeckel et al., 2004). Although our DCS results showed a significant right hemispheric predominance in the inferior parietal area under tactile sensation, we could not confirm it from the HG mapping analysis due to the insufficient number of subjects. Additionally, we were unable to construct functional maps of unexposed cortical regions such as the medial part of the S2, insula and cingulum due to the limited spatial coverage of the ECoG electrodes. Previous studies have suggested that DCS on these areas elicit various types of sensory-related experiences and that the medial S2 and insula are critically involved in tactile percep-

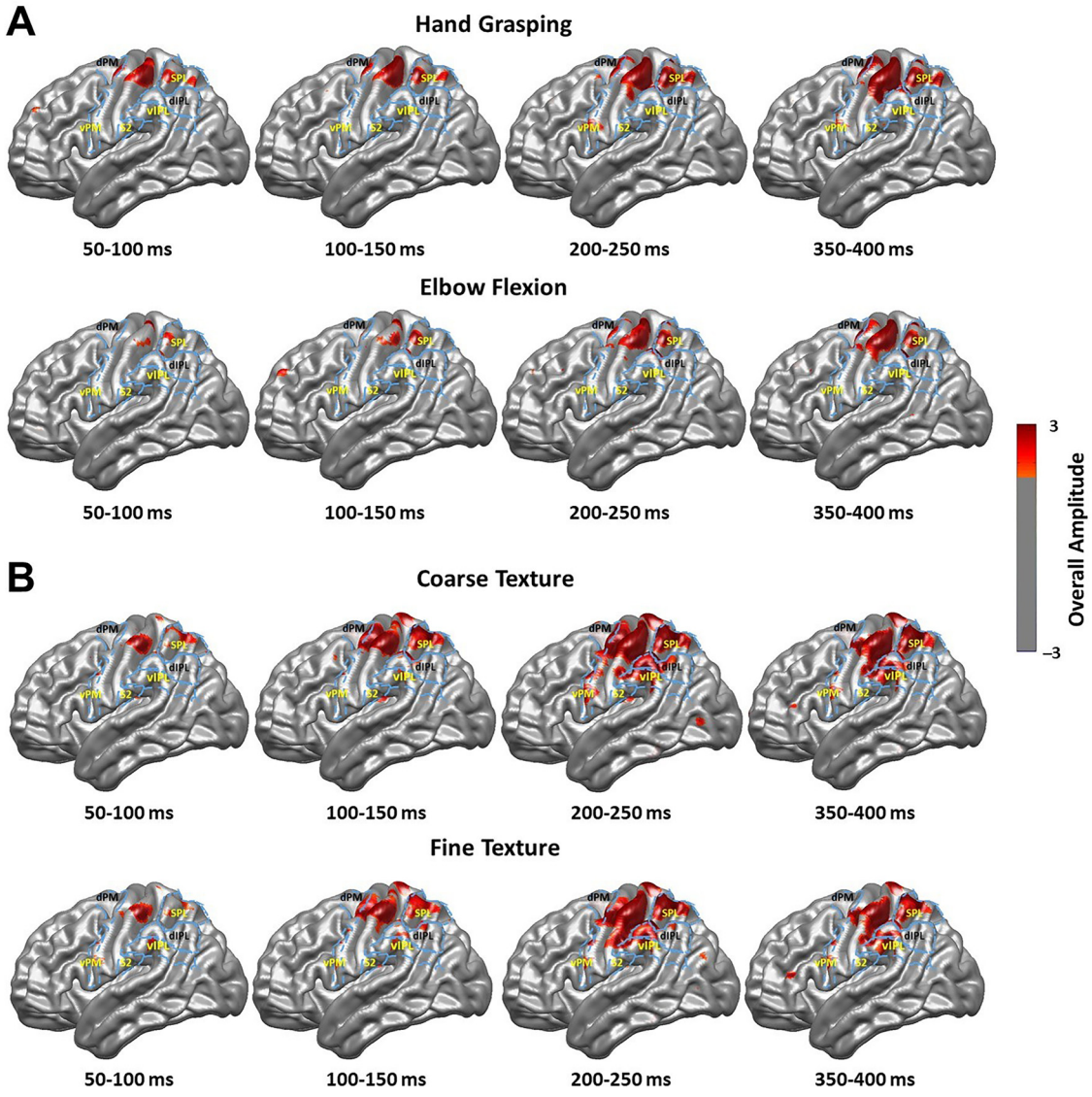

Fig. 7. Four-dimensional HG maps. Four-dimensional HG maps for (A) movement and (B) texture conditions. Cortical regions where significant HG activities were observed at each time bin were marked.

tion (Caruana et al., 2018; Preusser et al., 2015). Further investigation is needed to broaden the current map of somatosensory functions.

Previous magnetoencephalography (MEG) studies suggested that there exist narrow-band HG activities in the precentral area during movement (Cheyne et al., 2008; Muthukumaraswamy, 2010). Although ECoG is less sensitive to the tangential component of the cortical neural activity, we observed such narrow-band M1 activity in our previous ECoG study (Ryun et al., 2017a). Given the similarity between MEG and ECoG narrow-band HG activities, the dPM source (for movement) might be due to anterior activity or anterior activity in addition to more posterior precentral sulcal activity, the latter of which might be closely related to M1 sources that are picked up in MEG studies. However, considering that HG is a focal activity (Kaiju et al., 2021), the current results cannot directly confirm it. Further research would be warranted covering both dPM and M1 more densely. Additionally, in this study, we focused on the spatial delineation of power changes within a large HG band range. However, spectral characteristics of HG activities, such as the peak frequency and the frequency distribution, might differ between movement and tactile processing (see Supplementary Fig. 9). Further research is needed to investigate the spectral difference between movement and tactile processing.

In this study, we confirmed the hierarchical processing of tactile sensation by analyzing peak latency. Although we showed the temporal dynamics of movement-related HG activity and made direct comparisons between two conditions, we could not directly measure the hierarchical process of the movement-related condition due to the complexity of movement (hand grasping and elbow flexion motion). Further research focusing on the movement-related sensation is needed to clarify the hierarchical processing.

A recent ICMS study indicated that the quality of induced somatosensation was changed by the stimulus amplitude of the ICMS in the S1 area (Armenta Salas et al., 2018). In the present study, some patients reported sensory reports differently, depending on the type of stimulation (monopolar vs. bipolar), although such cases were very rare (14 electrodes). However, unlike the ICMS study, we were not able to directly change the stimulus parameters because the present research was retrospective. Further research is warranted to evoke various somatosensory qualities on the same electrode using DCS.

In this study, movement-related somatosensation elicited by DCS was determined by subjective patients' reports and visual inspection. Accordingly, it is possible that some movement-related somatosensations were not elicited by the intervention of the somatosensory system itself but

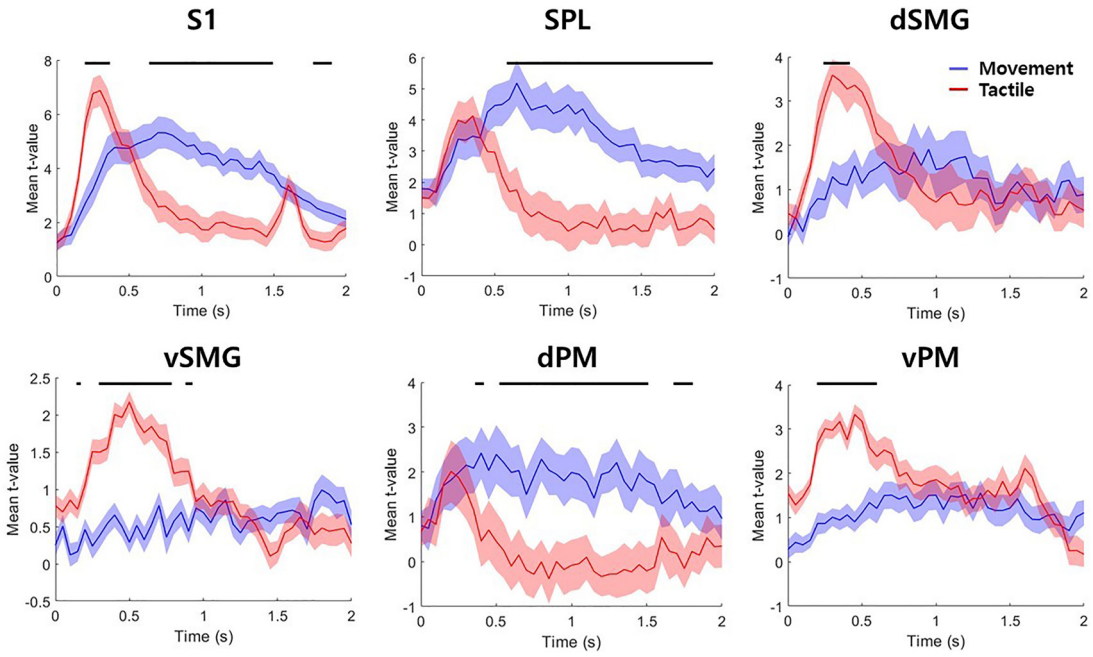

Fig. 8. Temporal dynamics of HG activity between movement (hand grasping + elbow flexion) and tactile (coarse + fine) conditions. Time series analysis of HG activities in S1 (hand/arm area), SPL, dSMG, vSMG, dPM and vPM. The shaded areas indicate the standard error of the mean (SEM). Black lines show significant periods within 0 to 2 s (FDR-corrected, $p < 0.05$).

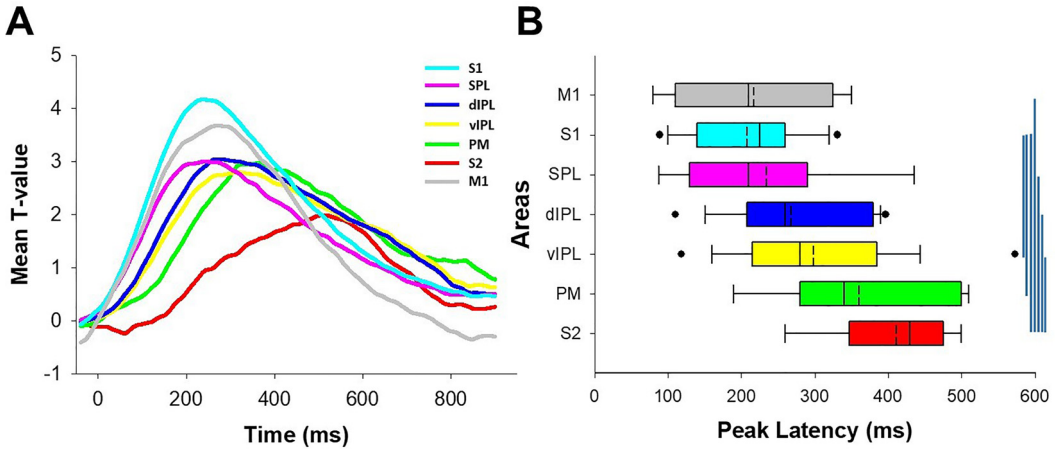

Fig. 9. HG temporal dynamics of each area. (A) Grand means of HG temporal dynamics in various somatosensory-related areas during fine texture stimulation. (B) HG peak latencies among areas in A from responsive electrodes of each ROI. Vertical blue lines indicate significant pairs (independent 2-sample *t*-test, Bonferroni corrected; $p < 0.05$). Dashed vertical lines indicate mean values.

by actual motor responses. Indeed, DCS on the posterior parietal cortex can induce motor responses because the PPC and M1 are densely interconnected (Gharbawie et al., 2011). Additionally, although we showed in the previous study that the movement-related HG activity in the somatosensory regions mainly represents feedback information from the periphery (Ryun et al., 2017a), the activity is possibly inflated by motor-related neural processing. Even considering these possibilities, however, their impacts on the present results would be limited because these issues are unrelated to the difference in the HG activity of the S2 and IPL regions between movement-related and tactile conditions.

The current findings provide some important insight into the bi-directional brain-machine interface (BMI) research incorporating somatosensory feedback by cortical stimulation. So far, studies on cortical stimulation for eliciting somatosensation have mainly focused on the S1 area because the stimulation on this area robustly induces somatosensory experiences of specific body parts. In the current study, we showed that DCS on high order cortical regions can induce somatosensory function-specific perceptual experiences depending on the location of the stimulation. This result may provide a cortical functional map for a multi-regional electrical stimulation to finely control the elicited sensation.

Declaration of Competing Interest

The authors declare that there are no competing financial interests regarding the publication of this paper.

Credit authorship contribution statement

Seokyun Ryun: Conceptualization, Data curation, Formal analysis, Investigation, Methodology, Software, Validation, Visualization, Writing – original draft. **Minkyu Kim:** Data curation, Formal analysis, Investigation, Writing – review & editing. **June Sic Kim:** Conceptualization, Methodology, Software, Writing – review & editing. **Chun Kee Chung:**

Conceptualization, Funding acquisition, Project administration, Supervision, Writing – review & editing.

Data availability

Data will be made available on request.

Acknowledgements

We thank Honggi Yeom for help with the ECoG experiments, and Mi Kyung Choe for providing MR and CT images. This research was supported by the Brain Research Program through the National Research Foundation (NRF) funded by the Ministry of Science and ICT (2016M3C7A1904984). This research was supported by the Alchemist Brain to X (B2X) Project funded by Ministry of Trade, Industry and Energy (20012355, NTIS: 1415181023).

Supplementary materials

Supplementary material associated with this article can be found, in the online version, at doi:10.1016/j.neuroimage.2023.120197.

References

Armenta Salas, M., Bashford, L., Kellis, S., Jafari, M., Jo, H., Kramer, D., Shanfield, K., Pejsa, K., Lee, B., Liu, C.Y., Andersen, R.A., 2018. Proprioceptive and cutaneous sensations in humans elicited by intracortical microstimulation. Elife 7.

Avanzini, P., Abdollahi, R.O., Sartori, I., Caruana, F., Pelliccia, V., Casaceli, G., Mai, R., Russo, G.L., Rizzolatti, G., Orban, G.A., 2016. Four-dimensional maps of the human somatosensory system. Proc. Natl Acad. Sci. 113, E1936–E1943.

Avanzini, P., Pelliccia, V., Lo Russo, G., Orban, G.A., Rizzolatti, G., 2018. Multiple time courses of somatosensory responses in human cortex. Neuroimage 169, 212–226.

Balestrini, S., Francione, S., Mai, R., Castana, L., Casaceli, G., Marino, D., Provinciali, L., Cardinale, F., Tassi, L., 2015. Multimodal responses induced by cortical stimulation of the parietal lobe: a stereo-electroencephalography study. Brain 138, 2596–2607.

Blankenburg, F., Ruff, C.C., Deichmann, R., Rees, G., Driver, J., 2006. The cutaneous rabbit illusion affects human primary sensory cortex somatotopically. PLoS Biol. 4, e69.

Breveglieri, R., Galletti, C., Gamberini, M., Passarelli, L., Fattori, P., 2006. Somatosensory cells in area PEc of macaque posterior parietal cortex. J. Neurosci. 26, 3679–3684.

Buneo, C.A., Andersen, R.A., 2006. The posterior parietal cortex: sensorimotor interface for the planning and online control of visually guided movements. Neuropsychologia 44, 2594–2606.

Callier, T., Suresh, A.K., Bensmaia, S.J., 2019. Neural coding of contact events in somatosensory cortex. Cereb. Cortex 29, 4613–4627.

Caruana, F., Gerbella, M., Avanzini, P., Gozzo, F., Pelliccia, V., Mai, R., Abdollahi, R.O., Cardinale, F., Sartori, I., Lo Russo, G., Rizzolatti, G., 2018. Motor and emotional behaviours elicited by electrical stimulation of the human cingulate cortex. Brain 141, 3035–3051.

Cheyne, D., Bells, S., Ferrari, P., Gaetz, W., Bostan, A.C., 2008. Self-paced movements induce high-frequency gamma oscillations in primary motor cortex. Neuroimage 42, 332–342.

Christensen, M.S., Lundbye-Jensen, J., Geertsen, S.S., Petersen, T.H., Paulson, O.B., Nielsen, J.B., 2007. Premotor cortex modulates somatosensory cortex during voluntary movements without proprioceptive feedback. Nat. Neurosci. 10, 417–419.

Delhaye, B.P., Long, K.H., Bensmaia, S.J., 2018. Neural basis of touch and proprioception in primate cortex. Compr Physiol 8, 1575–1602.

Desmurget, M., Reilly, K.T., Richard, N., Szathmari, A., Mottolese, C., Sirigu, A., 2009. Movement intention after parietal cortex stimulation in humans. Science 324, 811–813.

Dijkerman, H.C., de Haan, E.H., 2007. Somatosensory processes subserving perception and action. Behav. Brain Sci. 30, 189–201 discussion 201-139.

Disbrow, E., Litinas, E., Recanzone, G.H., Padberg, J., Krubitzer, L., 2003. Cortical connections of the second somatosensory area and the parietal ventral area in macaque monkeys. J. Comp. Neurol. 462, 382–399.

Eickhoff, S.B., Amunts, K., Mohlberg, H., Zilles, K., 2006. The human parietal operculum. II. Stereotaxic maps and correlation with functional imaging results. Cereb. Cortex 16, 268–279.

Flesher, S.N., Collinger, J.L., Foldes, S.T., Weiss, J.M., Downey, J.E., Tyler-Kabara, E.C., Bensmaia, S.J., Schwartz, A.B., Boninger, M.L., Gaunt, R.A., 2016. Intracortical microstimulation of human somatosensory cortex. Sci. Transl. Med. 8, 361ra141.

Freund, H.J., 2001. The parietal lobe as a sensorimotor interface: a perspective from clinical and neuroimaging data. Neuroimage 14, S142–S146.

Friedman, D.P., Murray, E.A., 1986. Thalamic connectivity of the second somatosensory area and neighboring somatosensory fields of the lateral sulcus of the macaque. J. Comp. Neurol. 252, 348–373.

Gamberini, M., Dal Bo, G., Breveglieri, R., Briganti, S., Passarelli, L., Fattori, P., Galletti, C., 2018. Sensory properties of the caudal aspect of the macaque's superior parietal lobule. Brain Struct. Funct. 223, 1863–1879.

Gardner, E.P., 2010. Dorsal and ventral streams in the sense of touch. Senses A Compr. Ref. 6, 233–258.

Gharbawie, O.A., Stepniewska, I., Kaas, J.H., 2011. Cortical connections of functional zones in posterior parietal cortex and frontal cortex motor regions in new world monkeys. Cereb. Cortex 21, 1981–2002.

Grafton, S.T., Fagg, A.H., Woods, R.P., Arbib, M.A., 1996. Functional anatomy of pointing and grasping in humans. Cereb. Cortex 6, 226–237.

Heed, T., Beurze, S.M., Toni, I., Roder, B., Medendorp, W.P., 2011. Functional Rather than Effector-Specific Organization of Human Posterior Parietal Cortex. J. Neurosci. 31, 3066–3076.

Hiremath, S.V., Tyler-Kabara, E.C., Wheeler, J.J., Moran, D.W., Gaunt, R.A., Collinger, J.L., Foldes, S.T., Weber, D.J., Chen, W., Boninger, M.L., Wang, W., 2017. Human perception of electrical stimulation on the surface of somatosensory cortex. PLoS One 12, e0176020.

Huang, M.X., Dale, A.M., Song, T., Halgren, E., Harrington, D.L., Podgorny, I., Canive, J.M., Lewis, S., Lee, R.R., 2006. Vector-based spatial-temporal minimum L1-norm solution for MEG. Neuroimage 31, 1025–1037.

Huttunen, J., Wikstrom, H., Korvenoja, A., Seppalainen, A.M., Aronen, H., Ilmoniemi, R.J., 1996. Significance of the second somatosensory cortex in sensorimotor integration: enhancement of sensory responses during finger movements. Neuroreport 7, 1009–1012.

Jancke, L., Kleinschmidt, A., Mirzazade, S., Shah, N.J., Freund, H.J., 2001. The role of the inferior parietal cortex in linking the tactile perception and manual construction of object shapes. Cereb. Cortex 11, 114–121.

Kaiju, T., Inoue, M., Hirata, M., Suzuki, T., 2021. High-density mapping of primate digit representations with a 1152-channelmicroECoG array. J. Neural Eng. 18.

Kamali, A., Flanders, A.E., Brody, J., Hunter, J.V., Hasan, K.M., 2014. Tracing superior longitudinal fasciculus connectivity in the human brain using high resolution diffusion tensor tractography. Brain Struct. Funct. 219, 269–281.

Kim, J.S., Singh, V., Lee, J.K., Lerch, J., Ad-Dab'bagh, Y., MacDonald, D., Lee, J.M., Kim, S.I., Evans, A.C., 2005. Automated 3-D extraction and evaluation of the inner and outer cortical surfaces using a Laplacian map and partial volume effect classification. Neuroimage 27, 210–221.

Lin, Y.Y., Simoes, C., Forss, N., Hari, R., 2000. Differential effects of muscle contraction from various body parts on neuromagnetic somatosensory responses. Neuroimage 11, 334–340.

Lyttelton, O.C., Karama, S., Ad-Dab'bagh, Y., Zatorre, R.J., Carbonell, F., Worsley, K., Evans, A.C., 2009. Positional and surface area asymmetry of the human cerebral cortex. Neuroimage 46, 895–903.

Matelli, M., Govoni, P., Galletti, C., Kutz, D.F., Luppino, G., 1998. Superior area 6 afferents from the superior parietal lobule in the macaque monkey. J. Comp. Neurol. 402, 327–352.

Murray, E.A., Mishkin, M., 1984. Relative contributions of SII and area 5 to tactile discrimination in monkeys. Behav. Brain Res. 11, 67–83.

Muthukumaraswamy, S.D., 2010. Functional properties of human primary motor cortex gamma oscillations. J. Neurophysiol. 104, 2873–2885.

Naito, E., Morita, T., Saito, D.N., Ban, M., Shimada, K., Okamoto, Y., Kosaka, H., Okazawa, H., Asada, M., 2017. Development of right-hemispheric dominance of inferior parietal lobule in proprioceptive illusion task. Cereb. Cortex 27, 5385–5397.

Nakai, Y., Jeong, J.W., Brown, E.C., Rothermel, R., Kojima, K., Kambara, T., Shah, A., Mittal, S., Sood, S., Asano, E., 2017. Three- and four-dimensional mapping of speech and language in patients with epilepsy. Brain 140, 1351–1370.

Nakai, Y., Nagashima, A., Hayakawa, A., Osuki, T., Jeong, J.W., Sugiura, A., Brown, E.C., Asano, E., 2018. Four-dimensional map of the human early visual system. Clin. Neurophysiol. 129, 188–197.

Padberg, J., Recanzone, G., Engle, J., Cooke, D., Goldring, A., Krubitzer, L., 2010. Lesions in posterior parietal area 5 in monkeys result in rapid behavioral and cortical plasticity. J. Neurosci. 30, 12918–12935.

Papademetris, X., Jackowski, M.P., Rajeevan, N., DiStasio, M., Okuda, H., Constable, R.T., Staib, L.H., 2006. BioImage Suite: an integrated medical image analysis suite: an update. Insight J 209.

Pause, M., Kunesch, E., Binkofski, F., Freund, H.J., 1989. Sensorimotor disturbances in patients with lesions of the parietal cortex. Brain 112 (Pt 6), 1599–1625.

Platz, T., 1996. Tactile agnosia. Casuistic evidence and theoretical remarks on modality-specific meaning representations and sensorimotor integration. Brain 119 (Pt 5), 1565–1574.

Preusser, S., Thiel, S.D., Rook, C., Roggenhofer, E., Kosatschek, A., Draganski, B., Blankenburg, F., Driver, J., Villringer, A., Pleger, B., 2015. The perception of touch and the ventral somatosensory pathway. Brain 138, 540–548.

Ray, S., Crone, N.E., Niebur, E., Franaszczuk, P.J., Hsiao, S.S., 2008. Neural correlates of high-gamma oscillations (60–200 Hz) in macaque local field potentials and their potential implications in electrocorticography. J. Neurosci. 28, 11526–11536.

Reed, C.L., Caselli, R.J., 1994. The nature of tactile agnosia: a case study. Neuropsychologia 32, 527–539.

Reed, C.L., Caselli, R.J., Farah, M.J., 1996. Tactile agnosia. Underlying impairment and implications for normal tactile object recognition. Brain 119 (Pt 3), 875–888.

Reed, C.L., Klatzky, R.L., Halgren, E., 2005. What vs. where in touch: an fMRI study. Neuroimage 25, 718–726.

Romo, R., Hernandez, A., Zainos, A., 2004. Neuronal correlates of a perceptual decision in ventral premotor cortex. Neuron 41, 165–173.

Rozzi, S., Calzavara, R., Belmalih, A., Borra, E., Gregoriou, G.G., Matelli, M., Luppino, G., 2006. Cortical connections of the inferior parietal cortical convexity of the macaque monkey. Cereb. Cortex 16, 1389–1417.

Rozzi, S., Ferrari, P.F., Bonini, L., Rizzolatti, G., Fogassi, L., 2008. Functional organization of inferior parietal lobule convexity in the macaque monkey: electrophysiological characterization of motor, sensory and mirror responses and their correlation with cytoarchitectonic areas. Eur. J. Neurosci. 28, 1569–1588.

Ryun, S., Kim, J.S., Jeon, E., Chung, C.K., 2017a. Movement-related sensorimotor high-gamma activity mainly represents somatosensory feedback. Front. Neurosci. 11, 408.

Ryun, S., Kim, J.S., Lee, H., Chung, C.K., 2017b. Tactile frequency-specific high-gamma activities in human primary and secondary somatosensory cortices. Sci. Rep. 7, 15442.

Ryun, S., Kim, J.S., Lee, S.H., Jeong, S., Kim, S.-P., Chung, C.K., 2014. Movement type prediction before its onset using signals from prefrontal area: an electrocorticography study. Biomed. Res. Int. 2014, 1–9.

Schmahmann, J.D., Smith, E.E., Eichler, F.S., Filley, C.M., 2008. Cerebral white matter: neuroanatomy, clinical neurology, and neurobehavioral correlates. Ann N Y Acad Sci 1142, 266–309.

Stoeckel, M.C., Weder, B., Binkofski, F., Choi, H.J., Amunts, K., Pieperhoff, P., Shah, N.J., Seitz, R.J., 2004. Left and right superior parietal lobule in tactile object discrimination. Eur. J. Neurosci. 19, 1067–1072.

Tomassini, V., Jbabdi, S., Klein, J.C., Behrens, T.E., Pozzilli, C., Matthews, P.M., Rushworth, M.F., Johansen-Berg, H., 2007. Diffusion-weighted imaging tractography-based parcellation of the human lateral premotor cortex identifies dorsal and ventral subregions with anatomical and functional specializations. J. Neurosci. 27, 10259–10269.

Westwood, D.A., Goodale, M.A., 2003. A haptic size-contrast illusion affects size perception but not grasping. Exp. Brain Res. 153, 253–259.

Xia, M., Wang, J., He, Y., 2013. BrainNet viewer: a network visualization tool for human brain connectomics. PLoS One 8, e68910.

Xiang, J., Hoshiyama, M., Koyama, S., Kaneoke, Y., Suzuki, H., Watanabe, S., Naka, D., Kakigi, R., 1997. Somatosensory evoked magnetic fields following passive finger movement. Brain Res. Cogn. Brain Res. 6, 73–82.